Journal of Nuclear Materials 562 (2022) 153586

Contents lists available at ScienceDirect

Journal of Nuclear Materials

journal homepage: www.elsevier.com/locate/jnucmat

Post-irradiation annealing of high flux irradiated and surveillance material reactor pressure vessel weld metal

Kristina Lindgren[a,*], Magnus Boåsen[b], Zaiqing Que[c], Krystyna Stiller[a], Pål Efsing[b,d], Mattias Thuvander[a]

[a] Department of Physics, Chalmers University of Technology, Göteborg SE-412 96, Sweden
[b] Solid Mechanics, Department of Engineering Mechanics, KTH Royal Institute of Technology, Stockholm SE-100 44, Sweden
[c] VTT Technical Research Centre of Finland Ltd, Espoo FI-020 44, Finland
[d] Vattenfall Ringhals AB, Väröbacka SE-430 22, Sweden

ARTICLE INFO

Article history:
Received 15 December 2021
Revised 4 February 2022
Accepted 6 February 2022
Available online 12 February 2022

Keywords:
Atom probe tomography
High flux
Irradiation hardening
Embrittlement
Post irradiation annealing
Clusters
Matrix defects

ABSTRACT

In this study, high flux irradiated and surveillance high Ni and Mn and low Cu welds identical to those of the belt-line region of Ringhals R4 were subjected to annealing at temperatures between 390 and 455 °C for 24–30 h, in order to study the dissolution of irradiation induced clusters and possible matrix defects using hardness testing and atom probe tomography. It was found that the cluster characteristics did not change during annealing at 390 °C, meaning that the size, number density and composition of the clusters, which mainly consist of Ni and Mn, did not change. Thus, the observed decrease in hardness during annealing of the high flux irradiated material is believed to be due to dissolution of matrix defects that were stable at the operating temperature. Cluster dissolution was observed after annealing at 410 °C in the high flux irradiated material, leaving around 10% of the original clusters. These clusters contained more Cu and less Ni and Mn than before annealing. The cluster dissolution at temperatures above 400 °C correlated with the decrease in hardness. The larger clusters of the surveillance material required a higher temperature or longer time to be dissolved compared to the clusters of the high flux material.

1. Introduction

During operation of a nuclear power plant, the reactor pressure vessel (RPV) is embrittled due to microstructural changes that are driven by neutron irradiation. The high-energy neutrons interact with the atom nuclei of the material, creating vacancies and interstitials. Most of the vacancies and interstitials recombine quickly, but some remain and subsequently cause the formation of nanometre-sized clusters containing Cu, Ni, Mn, and Si [1–3]. The clusters hinder dislocation movement, causing a hardening, and thereby contribute to embrittlement of the material. The clusters can be efficiently characterised by means of atom probe tomography (APT) [4–10]. The welds of the belt-line region get the highest exposure to neutron irradiation and are therefore most prone to cluster formation. As the RPV is considered to be a non-replaceable structure, and thereby possibly a life-limiting component of a nuclear reactor, it is vital to understand the long-term effects of operation on the RPV. It is also the most important component for the safety of a nuclear power plant.

Usually, a set of capsules containing surveillance material, representative of the RPV itself, is mounted at the internal structures of the RPV. This enables the removal of capsules at pre-determined intervals to assess the ageing-induced changes in the material, which has been exposed to higher fluence than the RPV due to the shorter distance to the reactor core. Thus, it gives a prediction of what will happen in the future to the RPV, assuming a low dependency of neutron flux on the microstructure development and the mechanical properties. The lead factor of surveillance materials is usually around 2–5, *i.e.,* the same fluence is achieved 2–5 times faster than in the RPV steel. Another way to simulate the degradation of the RPV is to use a materials test reactor (MTR). In this case, a significantly higher flux is usually used to reach the same dose level, as this decreases the time needed for exposure and gives the opportunity to start new ageing experiments long after the commissioning of the reactor. For MTRs the lead factors are much higher. The justification that these high fluxes affect the materials in a similar manner is crucial if the data are to be used for safety assessments. High flux irradiation to a similar fluence is

* Corresponding author.
E-mail address: kristina.lindgren@chalmers.se (K. Lindgren).

https://doi.org/10.1016/j.jnucmat.2022.153586

known to give smaller clusters with a higher number density than in surveillance material. Despite these differences, the degree of embrittlement is often similar after the same fluence [4,6,11,12], as the two effects approximately balance each other.

In addition to clustering of Ni, Mn, Si and Cu, matrix defects are known to form during irradiation of RPV welds and contribute to the hardening [2,13,14]. Matrix defects can be divided into stable matrix defects and unstable matrix defects, depending on their stability at reactor relevant temperatures. Unstable matrix defects are believed to both form and disappear at the reactor temperature, and thus their contribution to the hardening is expected to be larger at high flux neutron irradiation. However, the existence of unstable matrix defects at reactor relevant conditions is disputed [15–17]. Matrix defects consist of vacancies, small clusters of vacancies, interstitials, and combinations thereof [2]. For instance, they could be very small loops. Due to their small size, direct measurement such as by transmission electron microscopy (TEM) of these features is difficult or even impossible, and in many cases modelling or indirect measurements are used for their characterisation. Combining hardness measurements with post-irradiation annealing (PIA) is one way to approach this issue, and to simultaneously use characterisation techniques such as APT or small angle neutron scattering (SANS) to track changes in the clusters containing Ni, Mn, Si and Cu, also affecting the mechanical properties. Positron annihilation spectroscopy (PAS) can be used to study the behaviour of vacancies in the material during annealing [18]. PIA is also used to study the stability and dissolution of clusters, in order to further understand the cluster properties, and in some cases to regain mechanical properties by eliminating the clusters [19–22].

Archive material from Ringhals R4 RPV weld metal has been exposed to high flux irradiation, and subsequently it has been subjected to hardness and impact toughness testing as well as APT analysis [4,23]. The results of the mechanical testing of the high flux and the surveillance irradiated welds indicate that the hardening develops similarly in both cases, *i.e.,* along a similar trend line with respect to irradiation dose. The APT study by Lindgren et al. [4] revealed that the higher flux results in a higher number density of smaller clusters containing Ni, Mn, Si and Cu, contributing to the same increase in hardness as the lower flux (surveillance) irradiation. Furthermore, the same high flux irradiated welds and surveillance irradiated welds were annealed at 330 °C, 360 °C and 390 °C, and the hardness was measured at intervals of one hour, in order to study the presence of unstable matrix defects by Boåsen et al. [17]. Annealing at 330 °C and 360 °C did not affect the hardness of any of the materials. In the high flux material after annealing at 390 °C, a decrease in hardness was found that was not observed in the surveillance material. The different behaviours of the materials were attributed to the different cluster characteristics, assuming the dissolution of small clusters in the high flux material.

In this paper, the high flux irradiated Ringhals weld metal annealed at 390 °C is analysed using APT to study the cluster characteristics. Furthermore, the annealing study of the surveillance weld metal and the high flux Ringhals R4 weld metal is complemented using higher temperatures (up to 455 °C), and the cluster dissolution is studied using both hardness measurements and APT.

Table 2
The specimens' designation and the annealing conditions (temperature and time) and experimental techniques used (APT and/or time-resolved hardness (HV)). The designation "H6.4″ refers to Halden and the fluence of $6.4{\cdot}10^{23}$ n/m^2, and "S4.6″ to surveillance material irradiated to $4.6{\cdot}10^{23}$ n/m^2 as in previous investigations [4,17].

Name	Intended annealing temperature (°C)	Annealing time (h)	Experimental techniques
H6.4	-	-	APT, HV
H6.4–390	390	30	APT, HV
H6.4–400	405	24	APT, HV
H6.4–410	405	24	APT
H6.4–425	420	24	APT
H6.4–445	450	24	HV
H6.4–455	450	24	APT
S4.6	-	-	APT, HV
S4.6–390	390	30	HV
S4.6–400	405	24	HV
S4.6–445	450	24	APT, HV

2. Methods and materials

2.1. Materials

The weld metals studied were irradiated in high flux ($3.8{\cdot}10^{16}$ n/(m^{2}s), corresponding to a lead factor of around 75) to a fluence of $6.4{\cdot}10^{23}$ n/m^2 in Halden OECD MTR (Norway), and Ringhals R4 surveillance material irradiated to $4.6{\cdot}10^{23}$ n/m^2 (neutron flux $0.15{\cdot}10^{16}$ n/(m^{2}s), corresponding to a lead factor of around 3) [4,17,23]. The temperature during high flux neutron irradiation was 290–295 °C, and the surveillance material was irradiated in Ringhals 4 at 284 °C. The welds were subjected to a post weld heat treatment (PWHT) at 620 °C. The nominal composition is given in Table 1 together with the compositions as measured by APT of H6.4 (Halden $6.4{\cdot}10^{23}$) and S4.6 (Surveillance $4.6{\cdot}10^{23}$) including annealed materials. No significant difference in metal composition was observed before and after annealing. Due to the nature of the weld metal, some variation in composition is expected. S and Al are excluded from the measured values due to overlaps in the mass spectra with O_2^+, and Fe^{2+} and Cr^{2+}, respectively. The measured Cu content is higher in H6.4 (0.07%) than in S4.6 and the nominal value (both 0.04%).

In Table 2, the specimens and annealing times and temperatures are listed. Procedures of the annealing at 390 °C are described elsewhere [17]. In the cases the material was analysed by APT, it was done after the full annealing time. Two sets of annealing were performed for the higher temperatures. Annealing for APT at 405 °C, 420 °C, and 450 °C was performed in nitrogen atmosphere in a tube furnace at Chalmers. The annealing was in this case performed in one session of 24 h for each temperature. Annealing for hardness testing and APT at VTT were done at 405 °C and 450 °C in a tube furnace with pressurised helium. In this case, the annealing was stopped with some intervals, and then the material was hardness tested. For both furnaces used the temperature is expected to vary from the desired value with ± 5 °C. The annealing time of the H6.4–390 material was 30 h, whereas the other materials were annealed for 24 h. The reason of using different furnaces was mainly practical - the hardness measurements

Table 1
Chemical composition of the RPV weld in atomic%, nominal composition [24], as well as composition as measured by APT for H6.4 and S4.6 (average of all annealed materials). The error given is the standard deviation between the analyses.

at.%	C	Al	Si	P	S	Cr	Mn	Fe	Co	Ni	Cu	Mo
Nominal	0.31	0.05	0.28	0.027	0.007	0.04	1.37	Bal.	0.01	1.58	0.04	0.29
H6.4	0.07 ± 0.05	–	0.25 ± 0.05	0.01 ± 0.01	–	0.14 ± 0.08	1.08 ± 0.13	Bal.	0.02 ± 0.01	1.48 ± 0.16	0.07 ± 0.01	0.17 ± 0.08
S4.6	0.04 ± 0.03	–	0.28 ± 0.02	0.02 ± 0.01	–	0.15 ± 0.10	1.28 ± 0.15	Bal.	0.01 ± 0.01	1.64 ± 0.09	0.04 ± 0.01	0.21 ± 0.05

required a hot lab for safe handling of the radioactive material and were therefore done at VTT. However, annealing at Chalmers for APT was performed with small pieces of material and could thus be done in a safe way. When it turned out that the APT and hardness results differed, the VTT annealed pieces of material were sent to Chalmers for APT analysis. Thus, it was estimated that the furnace at Chalmers was up to 5 °C too warm, and the furnace at VTT was up to 5 °C too cold, both within the estimated error of the furnace temperatures. This explains the deviation between the temperature in the name (actual temperature) and the intended annealing temperature in Table 2.

2.2. Hardness testing

Hardness testing was carried out using a Struers Durascan 80 hardness tester at room temperature. Indentation was performed using a Vickers indenter and a 5 kgf load. All specimens displayed a significant hardness variability across the test surface. This was accounted for by mapping out the initial hardness across the specimen surface before any annealing heat treatments. This initial hardness was then used to reference the hardness difference. After each heat treatment, prior to hardness testing, the specimens were polished to remove any surface oxide that otherwise might skew the results. The methodology is described in detailed in [17].

2.3. APT

Specimen preparation for APT analysis was performed using a standard focused ion beam/scanning electron microscopy (FIB/SEM) lift-out technique, annular milling, and a final low-voltage mill to get rid of most ion damage and Ga ion implantation [25,26]. An FEI Versa 3D was used for this purpose.

An Imago LEAP 3000X HR, which has a detection efficiency of 37%, was used for the APT analysis of the materials. In addition to voltage pulsing (with high spatial resolution and giving good analysis of the Si and P distributions [27]), laser pulsing was used in order to obtain larger analysis volumes before fracture of the specimen. The analysis parameters were 60–70 K, 20% pulse fraction and 0.2% target evaporation rate for voltage pulsed analyses. Laser pulsing was done with a pulse energy of 0.30 nJ, temperature of 30 K and a target evaporation rate of 0.5–1.0%. In both cases the pulse frequency was 200 kHz. The APT data evaluation was done in the IVAS 3.6 software from Cameca.

Cluster analysis was performed using the maximum separation method (MSM) [28,29], where the 29 Da peak was excluded due to the $^{58}Ni^{2+}/^{58}Fe^{2+}$ overlap in accordance with [27]. After cluster identification, the 29 Da peak was decomposed and the Ni fraction was included in the cluster content. In order to avoid random matrix features being classified as clusters, cluster parameters and solute elements for the MSM were chosen differently dependant on the composition of the clusters. In the H6.4, H6.4–390, H6.4–400, S4.6 and S4.6–445 specimens, the clusters were defined by Ni (29 Da excluded) and Mn as solute elements, $d_{\max} = 0.50$ nm and $N_{\min} = 18$. In the H6.4–410, H6.4–425 and H6.4–455 specimens, these parameters often identified random variations in the matrix as clusters, due to the low cluster Ni and Mn content. Hence, Cu was used as solute element for cluster identification for these specimens, with $d_{max} = 1.0$ nm and $N_{min} = 8$. In all cases, the MSM parameters envelope distance and erosion distance were chosen equal to $d_{\max}$. In order to visualise clusters and dislocations, iso-concentration surfaces (isosurfaces) were used. These were constructed using a voxel size of 1.0 nm^3, with delocalization of $3.0 \times 3.0 \times 1.5$ nm^3.

APT analysis of the clusters in RPV steels is known to give cluster Fe contents that are higher than expected, and higher than what has been found using complimentary techniques such as TEM- and SANS [30–32]. In most clusters analysed in this paper, at least 50% of all atoms are identified as Fe. When cluster sizes and compositions are given, it is here assumed that Fe appearing in the clusters originates from local magnification effects [33]. This is supported by the unphysically high atomic density within the clusters in the APT reconstructions, which is caused by the low evaporation field of the clusters relative to the matrix. Hence, the cluster sizes were calculated from the number of Cu, Ni, Mn and Si atoms detected in the clusters, including the detection efficiency, and assuming matrix coherent clusters (thus, the volume per cluster atom is assumed to be equal to the volume per atom in bcc Fe). Cluster number densities were determined by counting the number of clusters in each analysis, whereby clusters cutting the edge of the analysis were counted as one half. Note that the actual crystal structure is unknown for the clusters due to the nature of APT data. Thus, the words cluster and precipitate are used interchangeably.

3. Results

3.1. Hardness measurements

The results from the combined PIA and hardness testing can be seen in Fig. 1. The results are presented as a difference ΔH_v, which has been calculated as the difference between the current hardness after each annealing heat treatment and a representative as-welded hardness that was calculated from the measurements presented in [17]. This means that a $\Delta H_v = 0$ relates to a hardness corresponding to no irradiation, around 216 HV5. The hardness values presented in Fig. 1 have been condensed by averaging the hardness from the indents before annealing and comparing to the average of the closest indents after annealing. The as irradiated hardness of H6.4 is around 288 HV5 and for S4.6 the hardness is 277 HV5. The ΔH_v values for as irradiated material are slightly lower, but in line with the values earlier published for these materials [4,17], owing to the inhomogeneous weld structure.

Annealing at the highest temperature, 445 °C, results in a significant decrease in hardness. In the high flux samples, H6.4, the hardness almost recovers fully after annealing at 24 h, while in the low flux samples, S4.6, the hardness is still not fully recovered at this point. Concerning the hardness after annealing at 400 °C, the hardness of the high flux samples decreases by $\Delta H_v = 24$ HV5, while in the low flux samples the decrease in hardness after 24 h of annealing is minute, similar to the behaviour at 390 °C. It should be noted that the results at 390 °C are the same as presented in [17] and are included here for completeness.

3.2. APT of high flux irradiated and annealed weld metal

3.2.1. General nanostructure

A reconstruction of a laser-pulsed APT analysis of material H6.4–390 can be seen in Fig. 2(a). There is a high number density of evenly distributed Ni-Mn-Si-clusters, visualised with Ni isosurfaces, within the entire reconstructed volume. A Mo-enriched dislocation, visualised with a red isosurface, is marked in the figure. On the dislocation, there are clusters sitting, with the same composition as the clusters in the matrix. In addition to Mo, the dislocation is also enriched in C and P (although this is a laser pulsed analysis, and thus the P is expected to diffuse on the surface prior to evaporation, there is still a clear P enrichment at the dislocation). Further down in the reconstruction, two more dislocations are cutting the edge of the analysis. The H6.4–390 material appears to be identical to the non-annealed H6.4 material [4], in terms of cluster characteristics. H6.4–400 has similar, but not identical clustering characteristics. This will be further elaborated below.

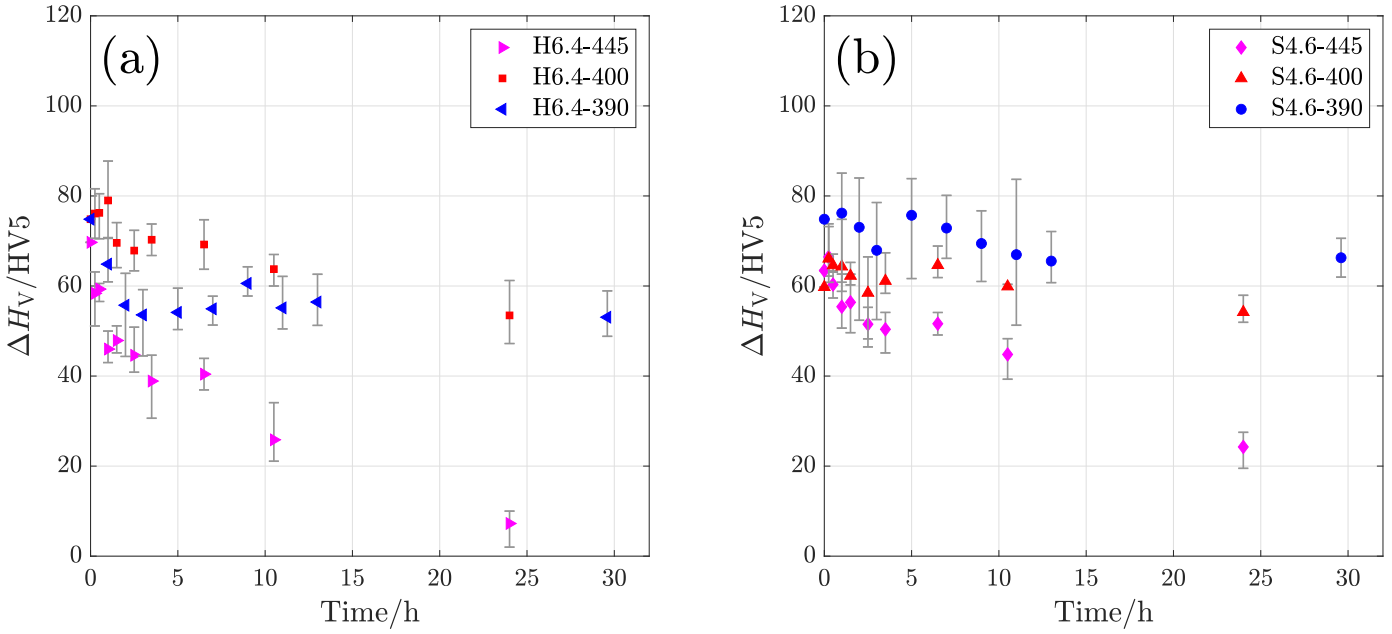

Fig. 1. Hardness as a function of annealing time at different temperatures for H6.4 in (a) and S4.6 in (b). The error bars are representative of the hardness range related to each coloured data point.

In Fig. 2(b), a reconstruction of a similar volume is shown, for H6.4–410. There is an obvious difference between this material and H6.4–390. Here, the number density of clusters is considerably lower and the distribution of clusters is uneven, leaving an empty volume in the middle of the reconstruction. The clusters that are left consist mainly of Cu instead of Ni and Mn, and are therefore visualised using Cu isosurfaces. Many of the clusters are located on dislocations, whereas some clusters appear to be in the matrix. Some of these matrix clusters are close to the edge of the analysis, while some are close to the centre. It is impossible to tell whether also these clusters are located on dislocations, as it is possible that not all dislocations contain segregants, such as Mo and C. APT does usually not give sufficient crystallographic information to identify dislocations unless they are decorated with segregating species.

Material H6.4–425 was found to be qualitatively similar to H6.4–410. The clusters found are located both on dislocations enriched in Mo and C, and sometimes without any apparent dislocation in the matrix. In material H6.4–455, a total of only three clusters were found, out of which none could be identified as being located on a dislocation, but two were on the edge of the analysis, opening for the possibility that they were actually located on dislocations passing right outside the analysis volume.

In all materials, occasional clusters containing some or all of the elements V, N, C and Cr were found. These often coincided with clusters of Ni-Mn-Si or Cu, or Mo-rich dislocations, but not always. These clusters are believed not to be affected by the irradiation, or the PIA, as they previously also have been found in reference materials and in thermally aged materials of similar composition [4,34,35].

3.2.2. Cluster characteristics

The cluster characteristics were found to vary depending on annealing temperature. In Fig. 3, the cluster number densities of the different materials are shown. There is no large difference between H6.4, H6.4–390, and H6.4–400. There is a significant difference between H6.4–400 and H6.4–410, indicating the difference in furnace temperature, although the intended temperature was the same, and a very sensitive temperature interval.

Table 3 gives the average cluster diameters and number densities. The difference between H6.4 and H6.4–390 number densities is believed to be insignificant, an effect of the heterogeneous weld, as the individual analysis results are within the same scatter interval. The H6.4–400 specimens have both a slightly lower average size and number density, resulting in a lower volume fraction than in H6.4–390. However, the H6.4–410 specimens have a number density that is one order of magnitude smaller than H6.4–400. The cluster size distributions have a cut-off for low sizes due to the N_{min} of the MSM, which might affect the average size slightly. There are no bimodal tendencies in the shapes of the size distributions (see supplementary material Fig. S1).

Table 3
Average cluster sizes (deduced from the number of Ni, Mn, Si, and Cu atoms) and number densities, with the standard deviation between analyses given as error.

Material	Average cluster diameter (nm)	Average cluster number density (10^{23}/m^3)	Cluster volume fraction (%)
H6.4	1.8 ± 0.1	5.9 ± 0.8	0.37
H6.4–390	1.8 ± 0.1	6.3 ± 1.6	0.41
H6.4–400	1.6 ± 0.1	5.6 ± 0.7	0.25
H6.4–410	1.5 ± 0.2	0.6 ± 0.2	0.02
H6.4–425	1.4 ± 0.2	0.2 ± 0.04	0.007
H6.4–455	1.3 ± 0.3	0.06 ± 0.04	0.001

The composition of the clusters was also found to vary between the different materials depending on annealing temperature. In Fig. 4, it can be seen that there is no obvious difference between the composition of the clusters in H6.4, H6.4–390, and H6.4–400. The Ni content is around 55%, Mn around 40%, and both Cu and Si are low (< 8%). For the Si content, only voltage pulsed analyses were used. H6.4–410, H6.4–425 and H6.4–455 contain much more Cu (60–80%) and less Ni and Mn (around 15% each). The cluster content of Si is 1% or less for the clusters in materials H6.4–410, H6.4–425 and H6.4–455. It is possible that the Si content is somewhat underestimated as laser pulsed analyses were used due to the low number density in these samples, and thus Si might have diffused on the surface prior to field evaporation.

Fig. 5 shows the total number of detected Cu atoms per cluster. Note that the detection efficiency of 37% is not used to adjust the

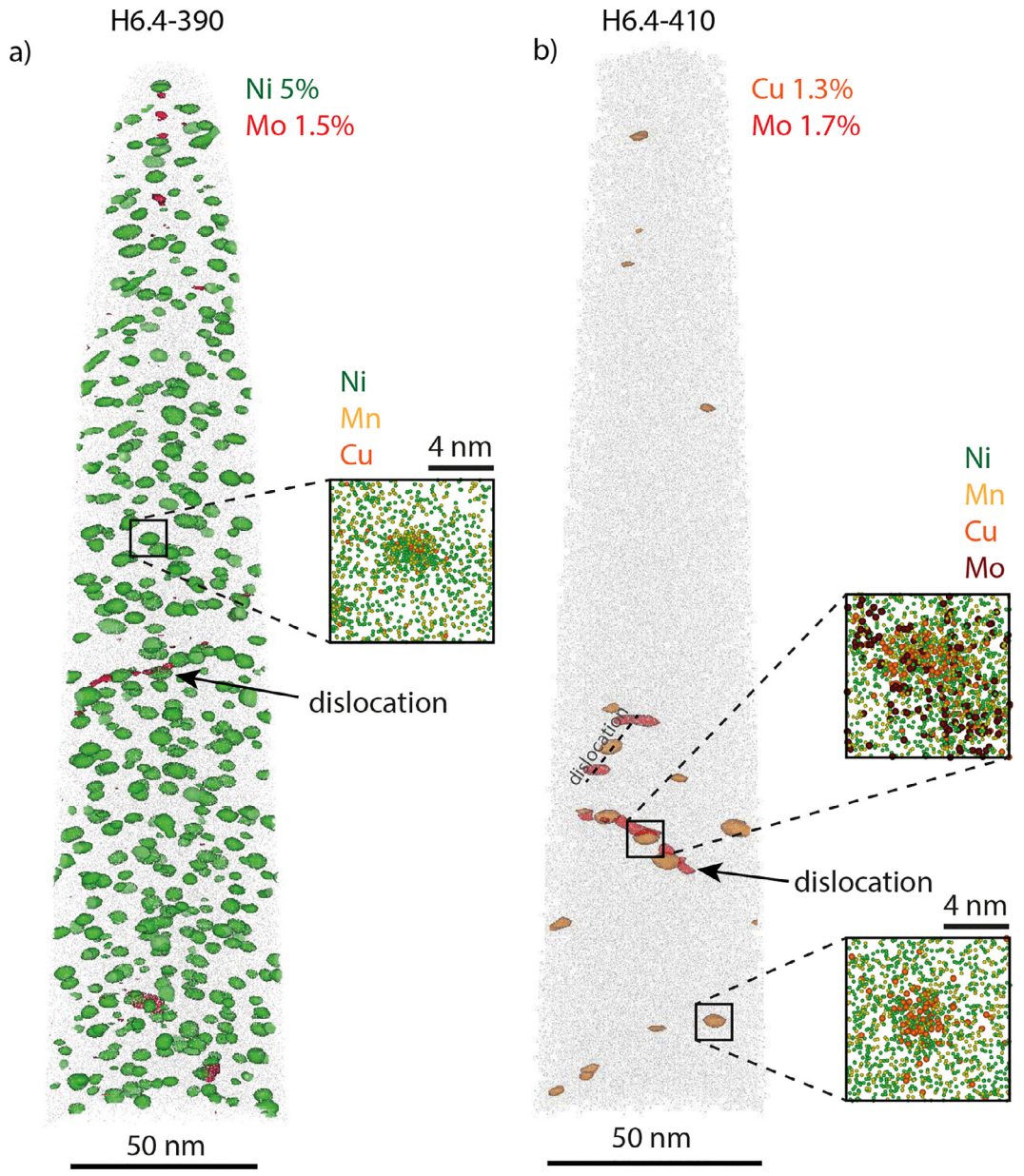

Fig. 2. (a) Material H6.4–390. Green isosurfaces correspond to 5% Ni and red isosurfaces to 1.5% Mo. Grey shows the extent of the analysis. Cluster cut out: 10 × 10 × 10 nm^3 box, green dots are Ni atoms, yellow are Mn and orange are Cu. (b) Material H6.4–410. Orange isosurfaces correspond to 1.3% Cu, red to 1.7% Mo. Grey shows the extent of the analysis. The boxes are 10 × 10 × 10 nm^3 and Ni atoms are green, Mn yellow, Cu orange and Mo dark brown.

numbers, *i.e.*, the actual numbers of atoms are larger. The graphs of H6.4–410, H6.4–425 and H6.4–455 have a higher cut-off at 8 (N_{min}) due to the cluster definition used (at least 8 Cu atoms are needed, whereas the clusters of H6.4, H6.4–390, and H6.4–400 are defined by Ni and Mn atoms). In material H6.4, H6.4–390, and H6.4–400, most of the clusters contain less than 20 Cu atoms. None of these clusters contain more than 50 Cu atoms (corresponding to 135 atoms when compensating for detection efficiency), and many contain no Cu atom at all. In H6.4–410, the number of Cu atoms per cluster has increased significantly. In fact, the largest two clusters are outside the size range of the graph (due to space limitations and comparability of the graphs), and contain 250 and 375 Cu atoms, respectively (676 and 1014 atoms when correcting for detection efficiency). After annealing at 425 °C, there are not as many clusters containing a large number of Cu atoms left. In material H6.4–455, the three clusters left contain 11, 33, and 51 detected Cu atoms (30, 89, and 138 corrected Cu atoms). Clusters on the edges are not removed from this analysis, and thus some of the clusters in the graphs might have been truncated.

In Fig. 6, the total solute contents of Ni, Mn and Cu are compared with the matrix solute contents, to illustrate the degree of clustering. The total content subtracted by the matrix content is found to vary between analyses of the same material, but usually the variations are within one order of magnitude. From Fig. 6, there is no difference between non-annealed material and the material annealed at 390 °C regarding Ni, Mn and Cu. In material H6.4–400, the annealing causes some Ni and Mn to dissolve into the matrix. Although there are large variations between analyses of the same material condition, and the absolute difference between total and matrix content is small, the amount of Ni and Mn in the clusters is decreasing from 410 °C to 455 °C. The Cu shows a similar trend as Ni and Mn, but at higher temperatures, except for H6.4–400, where more Cu atoms appear to be in the matrix than in H6.4–410. The reason for this is unknown at this point. The to-

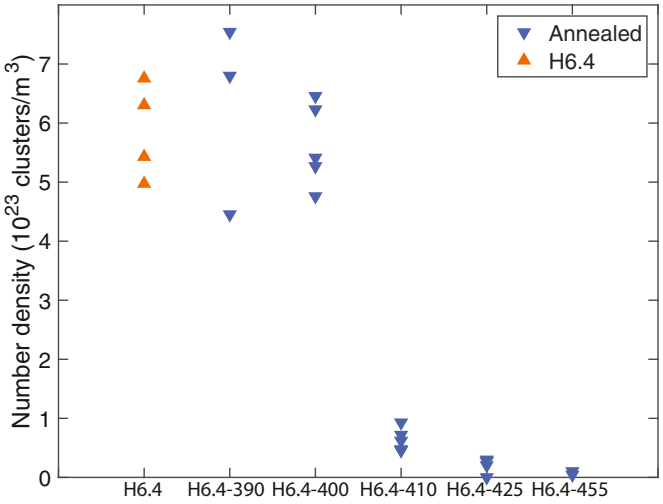

Fig. 3. Cluster number density for all the analysed materials from H6.4. Each marker represents one APT analysis.

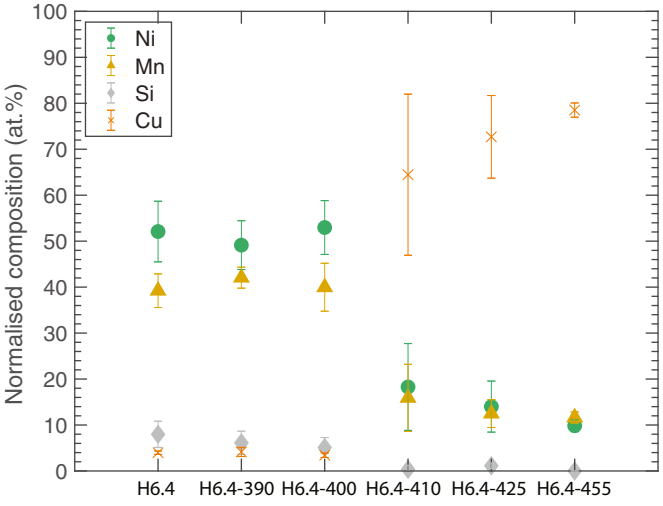

Fig. 4. Normalised cluster compositions, Fe removed. Standard deviations of clusters within each category are given as error bars.

tal contents of Ni, Mn, and Cu, as well as the matrix contents that were used to calculate these numbers are given in Fig. S2 in the supplementary material. For all elements, only a small fraction of the total number of atoms are found in the clusters.

3.3. APT of irradiated and annealed surveillance weld metal

Since the hardness of the 24 h annealed surveillance material (S4.6–445) was found to have not recovered to unirradiated levels, this material was also analysed using APT. The annealed material does contain a significant number of clusters, as can be seen in Table 4, including cluster diameter, number density and volume fraction. In Fig. 7, the size distributions and cumulative size distributions can be seen. After annealing, there appears to be a slightly higher percentage of clusters in the lower part of the size

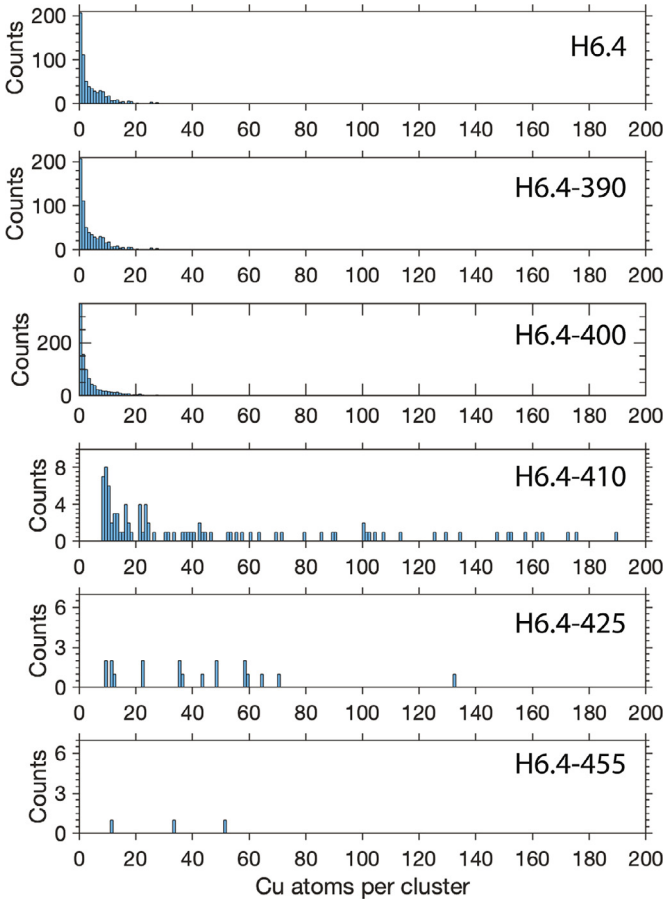

Fig. 5. Number of detected Cu atoms per cluster. Note that different cluster definitions give different cut-off at low values. Two clusters in H6.4–410 contained more than 200 Cu atoms (250 and 375, respectively) and are not shown. The number of Cu atoms is not corrected for the detection efficiency of the instrument (37%).

range. There are also clusters that are larger than 5 nm in diameter, which were not observed prior to annealing.

The normalised composition of these clusters is 51% Ni, 40% Mn, 7% Si, and 1.7% Cu both before and after annealing. In Fig. 8, the total amounts of Ni, Mn, and Cu minus the matrix content of the same elements are given. It can be seen that both Ni and Mn leave the clusters during the annealing, in line with the high flux material above. The Cu results have more scatter, but the average value indicates that also Cu atoms have left clusters. Overall, this results in the similar cluster composition before and after annealing. The total contents of Ni, Mn, and Cu, as well as the matrix contents that were used to calculate these numbers are given in Fig. S2 in the supplementary material. For Ni, Mn, and Cu, only a small fraction of the total number of atoms are found in the clusters.

4. Discussion

4.1. Behaviour of clustering elements in the high flux material during PIA

In this study, Ringhals R4 weld metal irradiated at high neutron flux and to a high fluence was annealed at different temperatures;

Table 4
Average diameter, number density and volume fraction of the surveillance material.

Material	Average cluster diameter (nm)	Average cluster number density (10^{23}/m^3)	Cluster volume fraction (%)
S4.6	2.4 ± 0.1	3.2 ± 1.1	0.50
S4.6–445	2.5 ± 0.1	1.6 ± 0.8	0.31

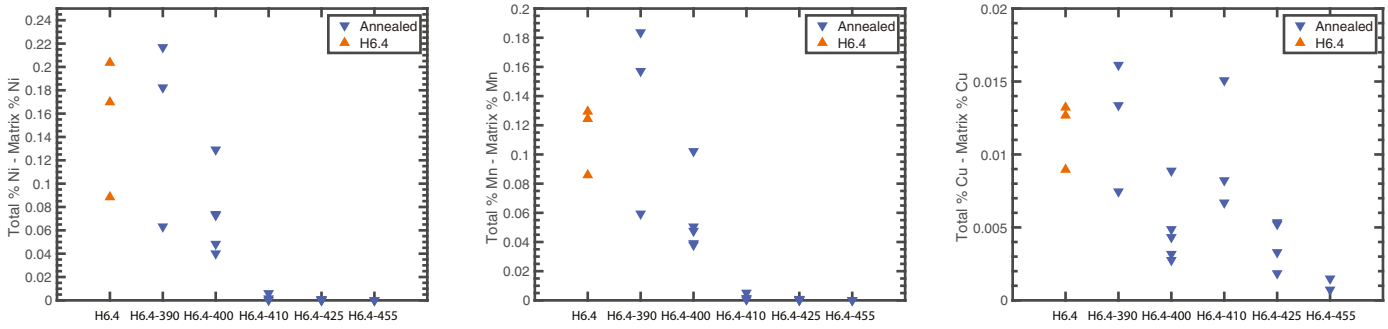

Fig. 6. The difference between total solute content and the matrix solute content for Ni, Mn, and Cu for the different high flux irradiated materials.

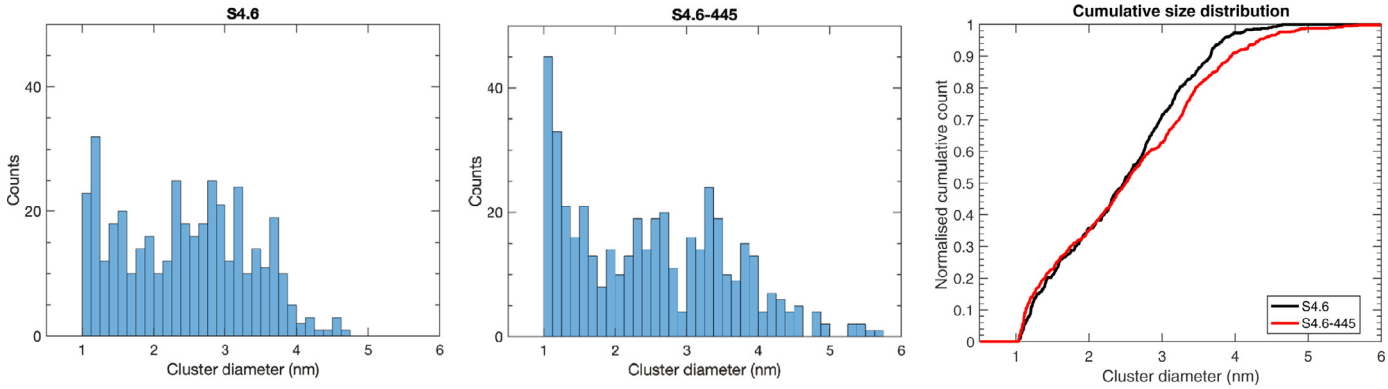

Fig. 7. Size distributions and normalised cumulative size distributions of S4.6 and S4.6–445.

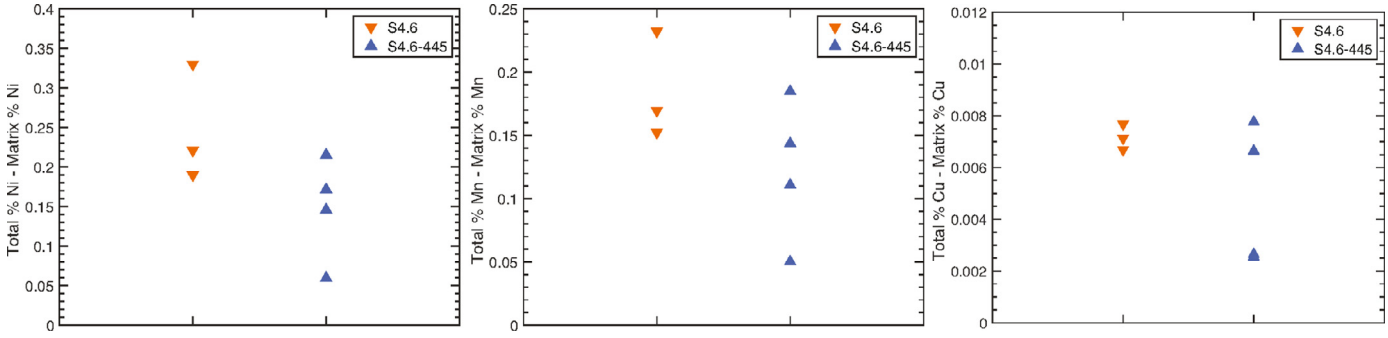

Fig. 8. The difference between total solute content and matrix solute content for Ni, Mn, and Cu for the surveillance material before and after annealing at 450 °C for 24 h.

390, 400, 410, 425, and 455 °C, for 24–30 h. Coupled to this, hardness measurements were performed. It was found that the annealing of H6.4 at 390 °C had no apparent effect on the cluster characteristics. The annealing at 400 °C and 410 °C resulted in very different cluster characteristics, indicating that this is a temperature range where the evolution of the structure is highly dependant on the exact temperature. In both cases, the clusters were dissolving, but to very different degrees. For material H6.4–410, the clusters were dissolving and the number density decreased by a factor of ten. Clearly, Ni, Mn and Si were dissolved into the matrix. The Cu atoms diffused to form Cu-rich precipitates, many on dislocations, whereas some appeared to be located in the matrix. Possibly the Cu-rich precipitates formed at the position of previous clusters, but this cannot be proven. Annealing at 425 °C led to dissolution of Cu as well into the matrix. After annealing at 455 °C, occasional Cu-rich clusters could still be found, but they had a very low number density, as well as a very low volume fraction.

The evolution of the clustering is in agreement with the hardness measurements, indicating a fully recovered hardness after annealing at 445 °C for 24 h (see Fig. 1). The results are in agreement with the results on model alloys by Bergner et al. [36], who did step-wise PIA of Fe-Cu, Fe-Mn-Ni and Fe-Mn-Ni-Cu at increasing temperatures. Using SANS, they found that the clusters dissolve at annealing temperatures above 400 °C, and that the Ni atoms in the Cu clusters were removed at the same temperatures, in accordance with the findings of this study. The low Cu content of the irradiated materials (H6.4) is expected to make PIA result in cluster dissolution rather than coarsening and growth [37].

The formation of Cu-rich clusters at 410 °C indicates thermodynamical stability of these features at this temperature. However, slightly higher temperatures dissolve these clusters as well. The materials annealed at and above 410 °C have some similarities with thermally aged material, like the Ringhals R4 pressurizer weld metal, where Cu-rich clusters with a Ni-Mn shell were found situated on dislocations [34,38]. However, the higher annealing temperatures (410 °C rather than 345 °C in the pressurizer) make Ni, Mn and Si dissolve to a larger extent, rather than go to the clusters as in the thermally aged pressurizer material.

There is no apparent compositional difference between the clusters in the matrix and those sitting on dislocations, neither before nor after annealing. However, number densities are affected - as can be seen in Fig. 2, the clusters on dislocations are sitting

closer to each other than the ones in the matrix, indicating that the matrix clusters dissolve to a larger extent than the clusters sitting on dislocations, which are more stable. Furthermore, the clusters sitting on dislocations have access to larger volumes through pipe diffusion, to attract Cu and grow.

4.2. Annealing at 390 °C - hardness and stable matrix defects

In the paper by Boåsen et al. [17], the hardness of the H6.4 material was measured during 30 h annealing at 390 °C. This corresponds to the hardness decrease from 288 HV5 down to 271 HV5, that is ∼24% of the irradiation induced hardness of as-irradiated H6.4, during the first three hours, as seen in Fig. 1. The hardness is still well above the unirradiated hardness of 216 HV. After this, the hardness changes were negligible. In the same paper, results from annealing of Ringhals surveillance weld metal were presented, but no decrease in hardness was found. This was speculatively attributed to dissolution of small clusters in the high flux material (H6.4), as it contains a higher number density of small clusters [4]. An alternative explanation would be the dissolution of matrix defects, which are stable at both 330 °C and 360 °C, but not at temperatures close to 390 °C. These matrix defects could for instance be clusters of vacancies, or loops without segregation (as reported in high flux irradiated alloys by Kasada et al. [39] and Bergner et al. [40]). Such matrix defects would exist to a larger extent in a high flux irradiated material due to the shorter time span of the irradiation. It is also possible that the clusters themselves could have different properties, for instance if the high flux-irradiated material contains clusters with more vacancies in them. The results presented in this paper show no difference in cluster characteristics before and after annealing at 390 °C (Figs. 3, 4, 5, and 6). Due to the heterogeneity of the welds, the error bars of the APT measurements are, however, large, making small changes hard to quantify. However, cluster dissolution has, unlike cluster formation, no energy barrier [41], and thus, the dissolution should happen to all Ni-Mn-Si clusters, until they are completely dissolved. The dissolution should not discontinue after a couple of hours at a hardness level that is much higher than in the unirradiated reference material. Here it is assumed that the solubility limit was not reached. Nagai et al. studied a dilute Fe-Cu model alloy using APT and PAS, and found that nanovoids dissolved after 30 min at 400 °C [42], supporting this theory. This is further supported by the PAS results by Konstantinovic et al., where stepwise annealing of Ringhals surveillance material for 30 min resulted in dissolution of vacancy clusters at 377 °C and dissolution of vacancy-Ni rich solute clusters at 477 °C [18]. The same authors also saw a significant decrease in hardness between the 30 min annealing at 450 °C and 500 °C, which is in line with the observations in this paper. Furthermore, Toyama et al. observed that there is an effect of flux on the vacancy behaviour and recovery of irradiated and annealed RPV weld metal [43].

It is possible that the materials irradiated in MTR contain matrix defects that are less stable than in the surveillance material, as proposed by Fukuya et al. [44]. Then, the matrix defects of the surveillance material would not dissolve at 390 °C, but at higher temperatures, when clusters are also dissolving, hiding their contribution to the hardness.

The 6 h longer annealing time of H6.4–390 in comparison to the other annealed materials does not make a significant difference, as there is no difference between this material and the non-annealed H6.4. In the hardness measurements by Boåsen et al. [17] the hardness decreased initially at 390 °C, but the hardness after 24 h and 30 h are estimated to be practically identical.

It is possible that other effects than dissolution of matrix defects and clusters could soften the material during the annealing, for instance a decreased C content of the matrix or decreased residual stresses. However, it is judged that these effects are small in comparison, since the 390 °C annealing of surveillance material did not result in any hardness recovery at all.

4.3. Behaviour of clustering elements in the surveillance material during PIA

The 24 h annealing of the R4 surveillance material gave slightly different results, compared to the results for high flux irradiation. The hardness measurements (Fig. 1) revealed a not yet fully recovered material after annealing at 445 °C for 24 h, and therefore the same material was analysed using APT, where a lower number density of clusters with similar sizes and compositions as before annealing were observed. However, the size distribution is slightly changed to contain both smaller and larger clusters.

The influence of annealing of Ringhals R3 surveillance weld metal was characterised by APT by Styman et al. [45]. The material was irradiated to a higher neutron fluence ($6.8{\cdot}10^{23}$ neutrons/m^3, neutron flux $1.5{\cdot}10^{14}$ neutrons/(m^2s)) than the surveillance material in this paper, and contained slightly larger clusters (average diameter 3.5 nm) with a number density that was 30% higher than in the surveillance material S4.6, but apart from that the materials were very similar. Annealing for 30 min at 450 °C resulted in a changed cluster size distribution. After additionally 10 min at 500 °C the average size of the clusters was smaller. It was observed that Mn was leaving the clusters first. The nature of the clusters after annealing at higher temperature is similar to what is found in this paper after longer time, clusters partly dissolved but show a similar composition after annealing.

It is possible that the lower Cu content (0.04 at.% as compared to 0.07 at.%) causes the difference in Cu composition of the clusters after annealing of S4.6 and H6.4. This can be interpreted in the way that the stability of Cu clusters is dependant on the Cu content [37] and the lower Cu content in the surveillance material compared to the high flux irradiated material could possibly result in a lower stability of Cu-rich clusters. It is also possible that Cu-rich clusters are not formed during the annealing of the surveillance material having something to do with the slower dissolution of Ni, Mn and Si from the clusters, that is an effect of the different neutron flux during irradiation.

A difference between H6.4–455 and S4.6–445 was the fact that the clusters in the high flux irradiated material were (close to) entirely dissolved after 24 h, whereas there was still a substantial number of clusters left in the surveillance material. However, there is a decreasing trend in the hardness curve. There is the possible effect of the different furnace temperatures and interruptions in the annealing when measuring hardness, but also the cluster size (2.4 nm and 1.8 nm diameter), that could be possible explanations of this phenomena. Another possibly contributing factor is a higher number of vacancies in the clusters in the high flux material, giving a faster dissolution than in the surveillance material.

5. Conclusions

In the annealing studies of surveillance and MTR irradiated Ringhals weld metal it was found that:

- The high flux irradiated material is fully recovered after 24 h annealing at 445 °C, but the surveillance material still has some clusters remaining, contributing to the hardness after the same annealing. This difference in cluster dissolution is tentatively attributed to the larger clusters and possibly fewer vacancies in the clusters of the surveillance material.
- Not only does the high flux irradiated material contain a higher number density of smaller clusters containing mainly Ni and Mn, the annealing studies also indicate a slightly higher contribution to hardness from so called matrix defects.

- The contribution to the hardness from these defects anneals out at roughly 390 °C in the high flux irradiated material.
- Annealing the high flux irradiated material at temperatures of at least 410 °C resulted in dissolution of Ni and Mn into the matrix, but left Cu rich clusters with a number density one order of magnitude lower than before annealing in the material.
- It was found that the exact annealing temperature in the interval 400–410 °C had a large impact on the high flux irradiated material. Annealing at 400 °C resulted in partial dissolution within the 24 h time frame studied, and not fully recovered hardness, as opposed to the significantly lower number density of clusters after 410 °C annealing for 24 h.

Declaration of Competing Interest

The authors declare that they have no known competing financial interests or personal relationships that could have appeared to influence the work reported in this paper.

CRediT authorship contribution statement

Kristina Lindgren: Investigation, Formal analysis, Visualization, Conceptualization, Writing – original draft, Writing – review & editing, Funding acquisition. **Magnus Boåsen:** Investigation, Conceptualization, Writing – original draft, Writing – review & editing, Funding acquisition. **Zaiqing Que:** Writing – review & editing. **Krystyna Stiller:** Supervision, Writing – review & editing. **Pål Efsing:** Funding acquisition, Conceptualization, Writing – review & editing. **Mattias Thuvander:** Conceptualization, Supervision, Writing – review & editing, Funding acquisition.

Acknowledgements

This investigation has been funded by the Swedish Radiation Safety Authority (SSM), as well as by the Swedish Centre for Nuclear Technology (SKC), and Nordic Nuclear Safety Research (NKS). Contribution to the funding also comes from the EU project ENTENTE (No 900018).

Ringhals is acknowledged for providing the materials. VTT is acknowledged for help with annealing, cutting and sending specimens. APT was performed in Chalmers Materials Analysis Lab (CMAL). Jari Lydman, Johanna Lukin, and Petteri Lappalainen at VTT are acknowledged for help with the annealing and hardness measurements of active specimens. Ulla Ehrnstén and Noora Hyttönen at VTT, as well as Jenny Roudén at Ringhals, are acknowledged for fruitful discussions. Burcak Ebin at the Department of Chemistry and Chemical Engineering at Chalmers is acknowledged for assistance by annealing.

Supplementary materials

Supplementary material associated with this article can be found, in the online version, at doi:10.1016/j.jnucmat.2022.153586.

References

[1] L. Messina, M. Chiapetto, P. Olsson, C.S. Becquart, L. Malerba, An object kinetic Monte Carlo model for the microstructure evolution of neutron-irradiated reactor pressure vessel steels, Phys. Status Solidi 213 (2016) 2974–2980.
[2] G.R. Odette, G.E. Lucas, Recent progress in understanding reactor pressure vessel steel embrittlement, Radiat. Eff. Defects Solids 144 (1–4) (1998) 189–231.
[3] J.C. van Duysen, G. Meric de Bellefon, 60th anniversary of electricity production from light water reactors: historical review of the contribution of materials science to the safety of the pressure vessel, J. Nucl. Mater. 484 (2017) 209–227.
[4] K. Lindgren, M. Boåsen, K. Stiller, P. Efsing, M. Thuvander, Evolution of precipitation in reactor pressure vessel steel welds under neutron irradiation, J. Nucl. Mater. 488 (2017) 222–230.
[5] E. Meslin, M. Lambrecht, M. Hernández-Mayoral, F. Bergner, L. Malerba, P. Pareige, B. Radiguet, A. Barbu, D. Gómez-Briceño, A. Ulbricht, A. Almazouzi, Characterization of neutron-irradiated ferritic model alloys and a RPV steel from combined APT, SANS, TEM and PAS analyses, J. Nucl. Mater. 406 (1) (2010) 73–83.
[6] N. Soneda, K. Nishida, A. Nomoto, K. Dohi, Flux effect on embrittlement of reactor pressure vessel steels irradiated to high fluences, in: Proceedings of the Fontevraud 8: Conference on Contribution of Materials Investigations and Operating Experience to LWRs' Safety, Performance and Reliability, Avignon, France, 2014.
[7] Y.I. Shtrombakh, B.A. Gurovich, E.A. Kuleshova, A.S. Frolov, S.V. Fedotova, D.A. Zhurko, E.V. Krikun, Effect of Ni content on thermal and radiation resistance of VVER RPV steel, J. Nucl. Mater. 461 (2015) 292–300.
[8] M.K. Miller, K.F. Russell, Embrittlement of RPV steels: an atom probe tomography perspective, J. Nucl. Mater. 371 (1–3) (2007) 145–160.
[9] M.K. Miller, K.A. Powers, R.K. Nanstad, P. Efsing, Atom probe tomography characterizations of high nickel, low copper surveillance RPV welds irradiated to high fluences, J. Nucl. Mater. 437 (1–3) (2013) 107–115.
[10] M. Shimodaira, T. Toyama, K. Yoshida, K. Inoue, N. Ebisawa, K. Tomura, T. Yoshiie, M.J. Konstantinović, R. Gérard, Y. Nagai, Contribution of irradiation-induced defects to hardening of a low-copper reactor pressure vessel steel, Acta Mater. 155 (2018) 402–409.
[11] A. Wagner, F. Bergner, R. Chaouadi, H. Hein, M. Hernández-Mayoral, M. Serrano, A. Ulbricht, E. Altstadt, Effect of neutron flux on the characteristics of irradiation-induced nanofeatures and hardening in pressure vessel steels, Acta Mater. 104 (2016) 131–142.
[12] K. Dohi, K. Nishida, A. Nomoto, N. Soneda, H. Matsuzawa, M. Tomimatsu, Effect of neutron flux at high fluence on microstructural and hardness changes of RPV steels, in: Proceedings of the ASME 2010 Pressure Vessels & Piping Division /K-PVP Conference, Bellevue, Washington, USA, 2010.
[13] G.R. Odette, E.V. Mader, G.E. Lueas, W.J. Phythian, C.A. English, The effect of flux on the irradiation hardening of pressure vessel steels, in: Proceedings of the Effects of Radiation on Materials 16th International Symposium, ASTM STP 1175, Philadelphia, 1993.
[14] M.G. Burke, R.J. Stofanak, J.M. Hyde, C.A. English, W.L. Server, Microstructural aspects of irradiation damage in A508 Gr 4N forging steel: composition and flux effects, J. ASTM Int. 1 (5) (2004) 194–207.
[15] R. Chaouadi, R. Gérard, Confirmatory investigations on the flux effect and associated unstable matrix damage in RPV materials exposed to high neutron fluence, J. Nucl. Mater. 437 (1–3) (2013) 267–274.
[16] R. Chaouadi, R. Gérard, Neutron flux and annealing effects on irradiation hardening of RPV materials, J. Nucl. Mater. 418 (1–3) (2011) 137–142.
[17] M. Boåsen, P. Efsing, U. Ehrnstén, On flux effects in a low alloy steel from a Swedish reactor pressure vessel, J. Nucl. Mater. 484 (2017) 110–119.
[18] M.J. Konstantinović, I. Uytdenhouwen, G. Bonny, N. Castin, L. Malerba, P. Efsing, Radiation induced solute clustering in high-Ni reactor pressure vessel steel, Acta Mater. 179 (2019) 183–189.
[19] P. Pareige, B. Radiguet, A. Suvorov, M. Kozodaev, E. Krasikov, O. Zabusov, J.P. Massoud, Three-dimensional atom probe study of irradiated, annealed and re-irradiated VVER 440 weld metals, Surf. Interface Anal. 36 (56) (2004) 581–584.
[20] M.K. Miller, K.F. Russell, Atom probe characterization of copper solubility in the Midland weld after neutron irradiation and thermal annealing, J. Nucl. Mater. 250 (1997) 223–228.
[21] P. Auger, P. Pareige, S. Welzel, J.C. Van Duysen, Synthesis of atom probe experiments on irradiation-induced solute segregation in French ferritic pressure vessel steels, J. Nucl. Mater. 280 (3) (2000) 331–344.
[22] N. Almirall, P.B. Wells, S. Pal, P.D. Edmondson, T. Yamamoto, K. Murakami, G.R. Odette, The mechanistic implications of the high temperature, long time thermal stability of nanoscale Mn-Ni-Si precipitates in irradiated reactor pressure vessel steels, Scr. Mater. 181 (2020) 134–139.
[23] P. Efsing, J. Roudén, P. Nilsson, Flux effects on radiation induced aging behaviour of low alloy steel weld material with high nickel and manganese content, Eff. Radiat. Nucl. Mater. 26 (2014) 119–134.
[24] P. Efsing, C. Jansson, T. Mager, G. Embring, Analysis of the ductile-to-brittle transition temperature shift in a commercial power plant with high nickel containing weld material, J. ASTM Int. 4 (7) (2007) 1–12 JAI100719.
[25] D.J. Larson, D.T. Foord, A.K. Petford-Long, H. Liew, M.G. Blamire, A. Cerezo, G.D.W. Smith, Field-ion specimen preparation using focused ion-beam milling, Ultramicroscopy 79 (1–4) (1999) 287–293.
[26] K. Thompson, D. Lawrence, D.J. Larson, J.D. Olson, T.F. Kelly, B. Gorman, *In situ* site-specific specimen preparation for atom probe tomography, Ultramicroscopy 107 (2–3) (2007) 131–139.
[27] K. Lindgren, K. Stiller, P. Efsing, M. Thuvander, On the analysis of clustering in an irradiated low alloy reactor pressure vessel steel weld, Microsc. Microanal. 23 (2) (2017) 376–384.
[28] D. Vaumousse, A. Cerezo, P.J. Warren, A procedure for quantification of precipitate microstructures from three-dimensional atom probe data, Ultramicroscopy 95 (2003) 215–221.
[29] J.M. Hyde, C.A. English, An analysis of the structure of irradiation induced cu-enriched clusters in low and high nickel welds, in: Proceedings of the Materials Research Society Symposium, Boston, 2000 R6.6.1-R6.6.12.
[30] A. Morley, G. Sha, S. Hirosawa, A. Cerezo, G.D. Smith, Determining the composition of small features in atom probe: bcc Cu-rich precipitates in an Fe-rich matrix, Ultramicroscopy 109 (5) (2009) 535–540.

[31] S. Shu, B.D. Wirth, P.B. Wells, D.D. Morgan, G.R. Odette, Multi-technique characterization of the precipitates in thermally aged and neutron irradiated Fe-Cu and Fe-Cu-Mn model alloys: atom probe tomography reconstruction implications, Acta Mater. 146 (2018) 237–252.
[32] P.D. Edmondson, C.M. Parish, R.K. Nanstad, Using complimentary microscopy methods to examine Ni-Mn-Si-precipitates in highly-irradiated reactor pressure vessel steels, Acta Mater. 134 (2017) 31–39.
[33] E.A. Marquis, J.M. Hyde, Applications of atom-probe tomography to the characterisation of solute behaviours, Mater. Sci. Eng. R Rep. 69 (4–5) (2010) 37–62.
[34] K. Lindgren, M. Boåsen, K. Stiller, P. Efsing, M. Thuvander, Cluster formation in in-service thermally aged pressurizer welds, J. Nucl. Mater. 504 (2018) 23–28.
[35] M. Boåsen, K. Lindgren, M. Öberg, M. Thuvander, J. Faleskog, P. Efsing, Analysis of thermal embrittlement of a low alloy steel weldment using fracture toughness and microstructural investigations, J. Nucl. Mater. 262 (2022) 108248.
[36] F. Bergner, A. Ulbricht, P. Lindner, U. Keiderling, L. Malerba, Post-irradiation annealing behavior of neutron-irradiated FeCu, FeMnNi and FeMnNiCu model alloys investigated by means of small-angle neutron scattering, J. Nucl. Mater. 454 (1–3) (2014) 22–27.
[37] A. Ulbricht, F. Bergner, C.D. Dewhurst, A. Heinemann, Small-angle neutron scattering study of post-irradiation annealed neutron irradiated pressure vessel steels, J. Nucl. Mater. 353 (1–2) (2006) 27–34.
[38] K. Lindgren, M. Boåsen, K. Stiller, P. Efsing, M. Thuvander, Thermal ageing of low alloy steel weldments from a Swedish nuclear power plant – the evolution of the microstructure, in: Proceedings of the Fontevraud 9: Contribution of Materials Investigations and Operating Experience to Light Water NPPs' Safety, Performance and Reliability, 2018.
[39] R. Kasada, T. Kitao, K. Morishita, A. Kimura, in: Effects of Copper Concentration and Neutron Flux on Irradiation Hardening and Microstructure Evolution in Fe-Cu Model Alloys, ASTM, 2001, pp. 237–246. STP 1405.
[40] F. Bergner, F. Gillemot, M. Hernández-Mayoral, M. Serrano, G. Török, A. Ulbricht, E. Altstadt, Contributions of Cu-rich clusters, dislocation loops and nanovoids to the irradiation-induced hardening of Cu-bearing low-Ni reactor pressure vessel steels, J. Nucl. Mater. 461 (2015) 37–44.
[41] R.W. Cahn, P. Haasen, Physical Metallurgy, 4th ed., North-Holland, Amsterdam, 1996.
[42] Y. Nagai, Z. Tang, M. Hassegawa, T. Kanai, M. Saneyasu, Irradiation-induced Cu aggregations in Fe: an origin of embrittlement of reactor pressure vessel steels, Phys. Rev. B 63 (13) (2001).
[43] T. Toyama, T. Yamamoto, N. Ebisawa, K. Inoue, Y. Nagai, G.R. Odette, Effects of neutron flux on irradiation-induced hardening and defects in RPV steels studied by positron annihilation spectroscopy, J. Nucl. Mater. 532 (2020).
[44] K. Fukuya, K. Ohno, H. Nakata, S. Dumbill, J.M. Hyde, Microstructural evolution in medium copper low alloy steels irradiated in a pressurized water reactor and a material test reactor, J. Nucl. Mater. 312 (2–3) (2003) 163–173.
[45] P.D. Styman, J.M. Hyde, D. Parfitt, K. Wilford, M.G. Burke, C.A. English, P. Efsing, Post-irradiation annealing of Ni–Mn–Si-enriched clusters in a neutron-irradiated RPV steel weld using atom probe tomography, J. Nucl. Mater. 459 (2015) 127–134.